Egypt. J. Chem. **Vol. 67,** No. 6 pp. 105 - 115 (2024)

Egyptian Journal of Chemistry
http://ejchem. journals.ekb.eg/

Synthesis of Nano-Hydroxyapatite Powder from Trough Clam Shells (Mactridae) by Wet Precipitation Method for Biomedical Applications

Sh. Hassanein[a], I.H. Ibrahim[a], Dina Salah[a], M. Sayed[b,*], S.M. Naga[b]

[a] *Physics Department, Faculty of Science, Ain Shams University, Cairo (Egypt)*

[b] *Refractories, Ceramics and Building materials Department, National Research Centre, 12622 El-Bohouth Str., Dokki, Cairo (Egypt)*

Abstract

The conversion of Trough Clam Shells waste into useful hydroxyapatite, through inexpensive eco-friendly methods has economic and environmental benefits. Hydroxyapatite (HAp), which has high bioactivity, excellent osseoconduction, and good biocompatibility, is the best choice for biomedical applications. In this work, trough clam shells (Mactridae) are used as a natural source containing beneficial elements for bone growth to produce nano-hydroxyapatite powder by the wet precipitation method through mixed the prepared 0.5 M of calcium hydroxide and 0.3 M of phosphoric acid. Then, sintered HAp discs were produced using a solid-state method at a sintering temperature of 1275 °C for 2 h. The produced HAp was characterized through X-ray diffraction (XRD), Scanning Electron Microscopy (SEM) coupled with Energy Dispersive X-ray Spectroscopy (EDS), Transmission Electron Microscopy (TEM), Thermogravimetric Analysis (TGA) and Fourier Transform Infrared Spectroscopy (FTIR) to determine the phase composition, morphology, particle size, thermal behavior and elemental composition, respectively. XRD and FTIR showed that the prepared powder is composed of pure hydroxyapatiteand possess a particle size ranging between 38.51 and 99.92 nm. SEM with EDS showed that HAp particles have semi- rounded shape together with a maintaining interconnected porosity of ≈ 5.3307%. The hardness and bending strengths were found to be ≈856.35 MPa and ≈38.73 MPa respectively. The bioactivity of prepared HAP is tested by immersing the samples in stimulated body fluid solution (SBF). The formation of a rich bone-like apatite layer on the disc's surface was detected after the immersion for 28 days. The prepared HAp was found to be suitable for bone tissue engineering.

***Keywords*:** Bioceramics; Clam shell; Hydroxyapatite; Mechanical properties; Bioactivity;

1. Introduction

Food and Agriculture Organization (FAO) found that shellfish aquaculture represents 42.6% of the total fish production [1]. The creation of these significant quantities of seashells is an important economic activity for many nations. The aquaculture industry generates around 6 to 8 million tons of garbage annually [2]. Tens of millions of shells are produced as bio-waste annually. The decomposition of shellfish waste can lead to foul smells and an increase in microbial growth, which can result in the release of higher levels of CO_2. To combat pollution, recycling shellfish waste is necessary. Researchers have found innovative ways to produce valuable products from different types of shellfish, including oysters, mussels, clams, razor clams, scallops, abalones, crabs, shrimps, and lobsters [3]. Although all shellfish have similar chemical compositions, they vary in their ratios. Seashells contain high levels of calcium, which can be ground and calcined to produce calcium oxide (lime). Lime has several applications in the biomedical field, including conversion to tricalcium phosphate and hydroxyapatite [4]. Lime can also be used as a catalyst for biodiesel production and for removing phosphates from water [5,6]. In the present study, clam shells will be used especially trough clam shells (Mactridae). Mactridae is composed of 0.8% of silicon dioxide (SiO_2), 0.1% aluminium oxide (Al_2O_3), 97% calcium carbonate ($CaCO_3$), 0.1% magnesium oxide (MgO), 0.4% sodium oxide (Na_2O), 0.4% sulfur trioxide (SO_3), 0.1% sulfate (SO_4) and 1.1% other compounds [3]. According to the calcium ratio present in the clam shells, it has the highest percentage of calcium compared to other shellfish. To our knowledge, there are a few reports that deal with the conversion of Mactridae to hydroxyapatite. Lately, researchers have been utilizing biogenic waste materials to create bioceramics because of their advantageous qualities. These materials are non-carcinogenic, non-toxic, non-allergenic, widely available, renewable, and can be accepted by living organisms. Additionally, using them helps with recycling and preserving the environment. Biogenic waste materials are also a great source of calcium, which is useful for creating hydroxyapatite for various biomedical applications like bone grafts [7], drug delivery [8], scaffolding [9], and tissue engineering [10]. In modern times, hydroxyapatite can be obtained from different natural sources such as eggshells [11], sea shells [12], cockle shells [13], algae [14], corals [15], mammalian bones (like bovines [16], horses, camels, and pigs), fish bones [17], and

*Corresponding author e-mail: monasayed382@yahoo.com ;
Receive Date: 20 September 2023, Revise Date: 08 November 2023, Accept Date: 29 November 2023
DOI: 10.21608/EJCHEM.2023.236647.8647

limestone [18]. HAp can also be created chemically through different methods like sol-gel synthesis [19], hydrothermal transformation [20], wet chemical precipitation [21], microwave irradiation [22], emulsion and microemulsion techniques [23], mechanochemical process [24], template synthesis [25], electrodepositing technique [26], and ultrasonication process [27]. The chosen preparation method has a significant impact on the properties of the resulting HAp, specifically its morphology. Hydroxyapatite (HAp) is a compound with the chemical formula $Ca_{10}(PO_4)_6(OH)_2$ [28] . It has a Ca/P ratio of 1.67 [29] and is considered the major inorganic material with a structure similar to bone. Compared to other calcium phosphate compounds like tricalcium phosphate (TCP) and tetra calcium phosphate (TTCP), the phosphate group in HAp is more stable at a pH range of 4-12 and an ambient temperature [30]. It can be synthesized as bioceramics or combined with other compounds to form composites that enhance its properties. In biomedical applications, Hydroxyapatite (HAp) is a commonly used material due to its biocompatibility, bioactivity, biodegradability, non-inflammatory nature, thermodynamic stability in its crystalline state, and osteoconductive properties [31-34]. Synthetic HAp can be found in various forms, such as powders, micro-/nano-crystals, dense [35] or porous scaffolds/sheets/ceramics, thin films, and composites with glasses, metals [36], and polymers. This paper focuses on manufacturing dense HAp since the porous form is unsuitable for load-bearing. However, fully dense HAp is difficult to make. The manufacturing process of HAp involves two steps: shaping the powder using techniques like tape casting, slip casting, uniaxial pressing, cold isostatic pressing, and compaction in the presence of a magnetic field. Shaping is always followed by a sintering step. There are several sintering methods to choose from, including conventional sintering, hot pressing, hot isostatic pressing, spark plasma sintering [37], microwave process [38], hydrothermal sintering, vacuum sintering, and the two-step sintering method [39].

K. Dhanaraj , 2018, [40] used sea shells (*Anadaragranosa* shells) as raw material to get calcium carbonate for nanohydroxyapatite preparation by microwave assisted irradiation method. Poly ethyl glycol (PEG) and poly vinyl alcohol (PVA) are used to prevent nuclei formation. The results showed that the capped hydroxyapatite with PVA was more efficient than PEG which appears in decreasing the crystalline size. M. Zulhasif Ahmad Khiri, 2019, [41] used Arc clam shells as calcium source in hydroxyapatite preparation by wet chemical precipitation method. Then it was sintered at different temperatures from 200 to 1000 ^oC. It was found that by increasing the sintering temperature, the density, hardness, linear shrinkage and crystalline size increases and the porosity decreases. The results concluded that hydroxyapatite was prepared by sintering temperature 1000 ^oC and pH =10, it gives high hardness more than other conditions. G. Karunakaran, 2020 [42] used blue mussel (*Mytilus edulis*) as a bio-waste to elicit calcium source from it to prepare hydroxyapatite by microwave-assisted synthesis method and doped it by magnesium which the doping carried out under organic modifier (polyvinylpyrrolidone). The results showed that the prepared HA had hexagonal structure and observed that Mg-doped HA is non-toxic and has antibacterial activity. S. Hussain, 2021 [43] prepared hydroxyapatite from Indian clam shells by hydrothermal technique between 700 to 1100 ^oC . The results conducted to by increasing the heating time, the particle size increases due to the agglomeration of nano-HA grains and the shape changed from rods/needle to spherical shape. M. Harkat, 2022 [44] synthesized nano-crystalline hydroxyapatite from the bio-waste (*Strombidaestrombus*) seashells as a calcium source by wet chemical precipitation method. The results revealed that the prepared HA consisted of single phase with hexagonal structure. As mentioned in the previous studies, different species of sea shells are used as biowaste to produce hydroxyapatite powder. However, in our study we used new species of sea shells and it is widely available in Egypt to prepare hydroxyapatite powder and hydroxyapatite discs. Moreover, we make the needed measurements for biomedical applications such as mechanical and biological tests. To our knowledge no studies have been conducted on the production of hydroxyapatite powder or bodies through the use of clam shells (Mactridae) speicies by simple and inexpensive co-precipitation method.

In this study, sintered hydroxyapatite was fabricated from clam shells (Mactridae) using a wet chemical precipitation method and uniaxial pressing, followed by conventional sintering. The discs were fired at various temperatures between 1200°C and 1300°C to determine the ideal temperature for achieving low porosity and high density, which are important for improving mechanical properties like bending strength and hardness. The hydroxyapatite was characterized using several techniques, including XRD, TEM, FTIR, and SEM with EDX to examine its physical and morphology properties. Finally, the resulting sintered hydroxyapatite was tested in vitro to evaluate its bioactivity and biodegradability.

2. Materials and methods

2.1. Materials

Clam shells (Mactridae) were collected from fish store. Trough clam shells (mactridae) is belong to Kingdom: Animalia, Phylum: Mollusca, Class: Bivalvia, Order: Venerida, Superfamily: Mactroidea, Family: Mactridae [45]. Orthophosphoric acid, H_3PO_4 (85%) from s d Fine-Chem Limited, MUMBAI 400 030, Ammonia Solution max. 33% NH_3, extra pure from Riedel-deHaën, Sigma-Aldrich Laborchemikalien GmbH. D-30926 Seelze, distilled water. Reagent-grade NaCl, $NaHCO_3$, KCl, $Na_2HPO_4{\cdot}2H_2O$, $MgCl_2{\cdot}6H_2O$, $CaCl_2$, and Na_2SO_4. For stimulated body fluid preparation were buffered with TRIS-

HCl buffer trishydroxymethyl aminomethane ($(CH_2OH)_3CNH_2$) and hydrochloric acid (HCl).

2.2. Preparation of hydroxyapatite powder from clam shells

The collected clams shells were washed several times with tap water and then deionized water (DI) to remove any contaminated materials, boiled for 1h in DI water and dried at 100°C for one day, then calcined in the furnace at 900°C for two hours with a rate of 5°C/min. The temperature was maintained at 900°C for 2 hours to ensure all pigments and organic materials attached to shells were decomposed. The samples were left to cool overnight in the furnace chamber. CaO was produced after the calcination process. The produced CaO powder was preserved in a tight air desiccator to avoid its absorbance to moisture. Then, CaO powder is used for calcium hydroxide preparation directly. Firstly, 0.5 M of calcium hydroxide and 0.3 M of phosphoric acid were mixed to produce a hydroxyapatite precipitate. The phosphoric acid solution was added to the calcium hydroxide solution drop-by-drop with slow stirring at 70°C to get a 1.67 Ca/P ratio and maintain the pH of the solution at the range of 10.5-11 by adding ammonia solution. After the amount of phosphoric acid has been finished, the solution was left with vigorous stirring at 70°C for one hour. Then the cloudy solution was left at room temperature for 24 hours. The white precipitate was filtered and washed several times to get rid of the excess amount of ammonia. Then the precipitate dried in an oven at 110°C for 24 hours. The hydroxyapatite formation equation was described as the following equation:

$$10\ Ca(OH)2 + 6H3PO4 \longrightarrow Ca10(PO4)6(OH)2 + \ 18H2O$$

The dried powder was calcined at a temperature of 900°C of for 2 hours. Then, the calcined powder was ground by a ball mill at 300rpm for 2h and sieved with a 90 µm stainless steel sieve to get a homogenized powder. The powder was characterized by an X-ray Diffractometer (XRD), Fourier Transform Infrared Spectroscopy (FTIR), and Transmission Electron Microscopy (TEM).

2.3. Preparation of sintered hydroxyapatite discs

The obtained HAp powder was converted to discs of 10 mm diameter and 5 mm thickness by uniaxially pressing in a steel mould at room temperature using a universal testing machine with an applied pressure of 30 KN. The prepared discs were sintered at different temperatures ranging between 1200°, 1225°, 1250°, 1275° and 1300°C for two hours as a soaking time at the peak temperature with a heating rate of 5^0C/min in a static air electric oven. The processing scheme for hydroxyapatite bodies preparation is illustrated in Fig. 1.

2.4. Characterization

The major and trace elements of clam shells powder before calcination were recognized by using x-ray fluorescence XRF (PW2404 with 6 analyzing crystals) which depends on the emission of fluorescent x-ray from the material has been excited by high energy that is greater than the energy of bounding electron. A small quantity of finely grounded clam shells pre-calcination was used to analyze the change of its mass with the change of temperature by using thermogravimetric analysis TGA (Setaram, Francelab) which depends on continuously recording the change of mass during a specified time – temperature program. The phase composition of clam shells and prepared hydroxyapatite were analyzed by x-ray diffraction analysis (X`Pert PRO with secondary monochromator, Cu-radiation of wavelength (λ=1.542Å) at potential 45 Kv and current constant 35 mA and scanning speed 0.040/sec) which based on the scattering at the Bragg condition for each crystalline plane. The functional groups of the calcined hydroxyapatites powder were examined using Fourier transform infrared (ATR FTIR) spectroscopy mode, Bruker VERTEX 70 model which is based on the measurement of vibration of a molecule that excited by infrared radiation. The bonds between atoms absorbs the light at different frequencies. The particle size of calcined hydroxyapatite was investigated by transmission electron microscope TEM (JEOL, JEM2100-HR, Japan, Electron probe micro-analyzer) in which a beam of electrons transmits through an extremely thin specimen, and then interacts with the specimen when passing through it

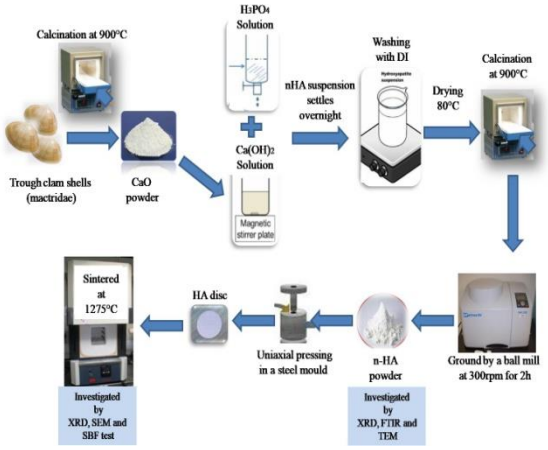

Fig.1. Processing scheme for hydroxyapatite bodies preparation.

.

The bulk density and apparent porosity were measured for sintered discs by applying the Archimedes method states that, when a body is immersed in a fluid system either wholly or partially, it is buoyed or lifted up by a force that is equal to the weight of the fluid displaced by the body (ASTM C-20) [46]. The discs that possess the highest density and the lower porosity were examined by X-Ray Diffractometer (XRD), and Scanning Electron Microscopy (SEM). The microstructure of hydroxyapatite before and after in vitro test was investigated by using a Scanning Electron Microscope attached to EDS (SEM Model XL 30, Philips, Eindhoven, Netherlands, with an attached EDX unit) which based on the generation of electron-hole pairs by the backscattered electrons which escape the sample and are absorbed by the detector. The bending strength was measured by a 3-point bending test on a universal testing machine (Model Tinius Olsen 25 ST, Honeycrock Land, Salfordsn Surrey RH15DZ, UK), with a crosshead speed of 0.01 mm/min). When a specimen is bent, it experiences a range of stresses across its depth. At the edge of the concave face of the specimen, the stress will be at its maximum compressive value. The hardness of sintered sample was carried out by using a hardness tester (Omnimet automatic MHK system Model Micro Met 5114, Buehler USA), use force a diamond spheroconical indenter under

specified conditions into the surface of the material and measure the difference in depth of the indentation.

2.5. In-vitro bioactivity estimation:

Bioactivity test

The stimulated body fluid (SBF) is a fluid which mimics the human body plasma in its ion concentrations. It was prepared by dissolving reagent grade chemicals of NaCl, $NaHCO_3$, KCl, $Na_2HPO_4{\cdot}2H_2O$, $MgCl_2{\cdot}6H_2O$, $CaCl_2$, and Na_2SO_4 in deionized water, and 50 mM tris buffer tris hydroxymethyl aminomethane $(CH_2OH)_3CNH_2$). 45 mM hydrochloric acid (HCl) was added as a buffer to the solution to keep the PH at 7.25. The prepared solution was maintained at 37°C throughout the preparation time [47]. The specimens were soaked in the stimulated body fluid for various periods (1, 3, 7, 14, 21, and 28 days) before being taken out and washed gently. Following these immersion times, inductively coupled plasma–optical emission spectrometry (ICP–OES) (5100 ICP–OES torch, Agilent, Australia) were used to analyze the solutions and determine the concentration of calcium and phosphorus ions. To confirm the data, each value was measured three times, and the average value was determined. The samples were characterized by SEM with EDX to show the formation of an apatite layer on its surface at the end of the immersion time.

Weight loss test

The degradation test was used for evaluating the weight loss (%) of the studied sintered HAp discs in 100 mL of TRIS-HCl buffer (Trizma base 0.05 M, NaCl 0.15 M, Sodium azide 0.01% w/v) at 37◦C (pH 7.4). the prepared discs were weighed before and after immersed in TRIS-HCl buffer for a various immersed time (1, 3, 7, 14, 21, 28 days). Weight loss% was carried for three measurements, and the mean value was taken to guarantee the accuracy of the measurement data

The weight loss (WL) was calculated according to the following equation [48]:

$$WL = \left[\frac{(W0 - Wt)}{W0}\right] x100$$

where W0 is the initial weight of sample and Wt the final weight of sample after soaking in Tris solution.

3. Results and discussion

3.1. Characterization of Trough clam shells:

The chemical composition of trough clam shells was analyzed using XRF, and the results are presented in Table 1. The analysis revealed that the shells are mainly composed of calcium oxide (55.48%). Additionally, during the calcination process, there was an ignition loss of 43.59% due to the decomposition of calcium carbonate ($CaCO_3$) and the release of carbon dioxide (CO_2). According to Table 1, trough clam shells contain various valuable trace elements in different ratios. The main components of these trace elements are strontium (Sr), zirconium (Zr), barium (Ba), and cobalt (Co). Strontium (Sr) is known to boost osteoblasts, inhibit osteoclasts, and improve bone strength [49]. Barium (Ba) plays a vital role in increasing apatite formation, enhancing bioactivity, and promoting good proliferation and viability of different cell lines [50]. Recent studies have shown that zirconia (ZrO_2) and Zr-ions stimulate the growth and development of human osteoblasts [51]. Some in-vitro studies have indicated that Co encourages angiogenesis and the growth of new bone [52, 53]. Although small amounts of cobalt (50-100 mol/L) enhance osteogenesis, higher levels of cobalt inhibit cell growth [54]. Other elements, such as lanthanum (La), rubidium (Rb), and zinc (Zn), are also present in small percentages.

According to the data, the levels of lead (Pb) and chromium (Cr), which are heavy metals, were found to be within safe limits that meet the specifications for ASTM F1538-03 biomaterials [55]. The prepared biomaterial should have controlled heavy metal concentration (ppm) like arsenic (As) less than 3 ppm, mercury (Hg) less than 5 ppm, cadmium (Cd) less than 5 ppm, and lead (Pb) less than 30 ppm. In the present study, there were no traces of (Hg), cadmium (Cd), and arsenic (As) found in the chemical composition of the trough clam shells.

Calcite, aragonite, and vaterite are three distinct polymorphic minerals of calcium carbonate. Although they share the same chemical structure, calcite and aragonite have different crystallinity. Figure 2 displays XRD pattern for clam shells, which are composed of calcium carbonate with an identified aragonite polymorph (JCPDS: 76-0606).

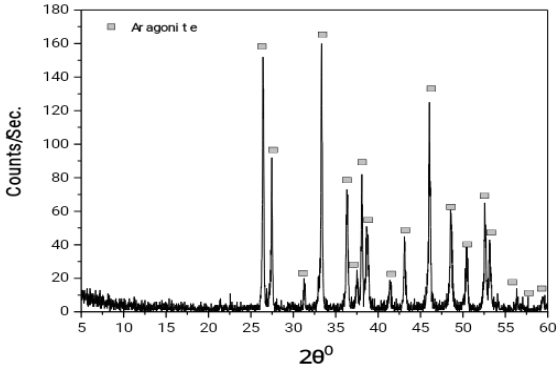

Fig.2. XRD pattern for trough clam shells powder.

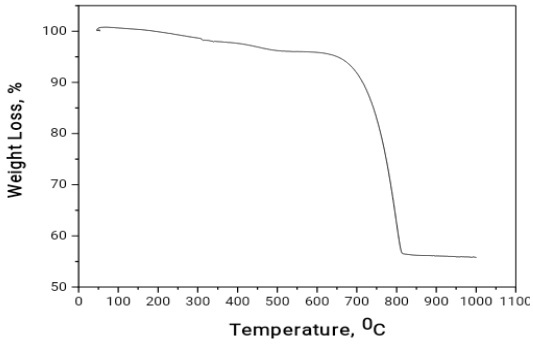

Fig.3. TGA graph for trough clam shells powder.

The idea of this method is obtaining high intensity scattered x-ray due to instructive interference which is resulted from bombardment by monochromatic x-ray. The following equation states Debye- Scherrer method [56]:

$$D = \frac{k\lambda}{\beta\, Cos\, \theta}$$

Where D: crystalline size of nano particles (nm), k: Scherrer constant =0.9, λ: the wavelength of x-ray source = 1.542Å, β: the full width at half maximum (FWHM) (radians), θ: peak position (radians).The result indicated that the average of the clam shell particles size obtained from XRD data is 36.87 ± 3.50 nm.

Table 1: XRF analysis of main oxides and trace elements for trough clam shells.

Chemical composition													
Main Oxide (wt.%)	CaO	SiO_2	SO_3	P_2O_5	Na_2O	TiO_2	Al_2O_3	MnO	MgO	K_2O	Cl	Fe_2O_3	L.O.I
	55.48	0.18	0.16	0.13	0.05	0.02	<0.01	<0.01	0.01	<0.01	<0.01	0.01	43.59
Trace Elements (PPM)	Sr	Zr	Ba	Co	La	Rb	Zn	Pb	V	Cr	Ni	Cu	Nb
	981.0	106	43.0	23.0	8.0	6.4	4.0	4.0	<2	<2	<2	<2	<2

Figure (3) displays the results of thermogravimetric analysis (TGA) for trough clam shells, from room temperature up to 1000^0 C. The calcium carbonate ($CaCO_3$) decomposition pattern exhibits two distinct stages. The first stage involves a minor weight loss between room temperature and 675^0 C, as a result of the removal of water and pigments present in the clam shells. The weight loss in this stage is approximately 6.1%. The second stage is observed at around 580˚C and ends at 815˚C. A rapid reduction in weight loss is detected between 700° and 900°C, due to the conversion of $CaCO_3$ contained in the clam shells into CaO, along with the removal of organic matter. In this stage, the weight loss drops and reaches about 36.2%. The weight of the clam shell remains consistent up to 900° C [57].

3.2. Characterization of the prepared hydroxyapatite powder from trough clam shells:

The XRD analysis of the prepared hydroxyapatite powder from trough clam shells by co-precipitation method at 900°C for 2 hours, is demonstrated in fig. 4. The diagram indicates that the powder was composed completely of hydroxyapatite phase matches with JCPDS (009 – 0432), without appearance of another secondary phase. The peak's strength and sharpness of the prepared HAp reflected high crystallinity development [58]. Moreover, the result indicated that the average particle size of the prepared HAp powder obtained from XRD data is 55.04 ± 11.78 nm.

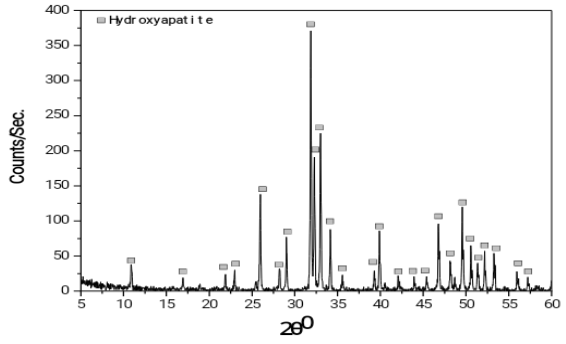

Fig.4. XRD patterns for hydroxyapatite powder calcined at 900°C.

Figure 5 displays the FTIR spectra of calcined hydroxyapatite powder scanned from 400 to 4000 cm^{-1}. The presence of $Ca_{10}(PO_4)_6(OH)_2$ components such as PO_4^{3-}, CO_3^{2-}, and OH^- are represented by bands in the spectra. The appearance of CO_3^{2-} is due to some compounds not transforming during sintering. The absorption bands of PO_4^{3-} in regions 473.92, 599.25, 563.47, 962.28, 1088.60, and 1021.27cm^{-1}, with symmetric stretching vibration[1] (P-O) existing for PO_4^{3-} exists at the frequency 962.28cm^{-1}.There are other various vibrations present in PO_4^{3-} such as the symmetric bending vibration[2] (P-O) at 473.92cm^{-1} and the asymmetric bending vibration 4 (P-O) at 599.25cm^{-1} and 563.47cm^{-1}. An absorption band of OH^- can be observed in the range of 629.69cm^{-1} as vibration mode and 3572.21cm^{-1} as stretching mode. Additionally, the presence of CO_3^{2-} stretching vibration mode is indicated by the absorption band at 1411.81cm^{-1}. Two unidentified bands in the spectra can be seen at the frequency of 430.27cm^{-1} and 673.72cm^{-1}. The FTIR results suggest that the main compound present is hydroxyapatite [59-61].

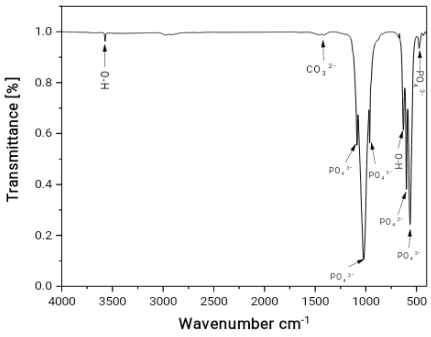

Fig.5. The FTIR of hydroxyapatite powder calcined at 900^0C.

The transmission electron microscope (TEM) for calcined hydroxyapatite at 900^0C is shown in Fig. 6a. It shows that hydroxyapatite has hexagonal and semi-rounded morphology. A dense agglomerated particle appears in the sample, whose particle size ranges between 38.51 and 99.92 nm. The selected area electron diffraction (SAED) pattern in Fig. 6b shows that hydroxyapatite powder possesses a well-crystalline structure.

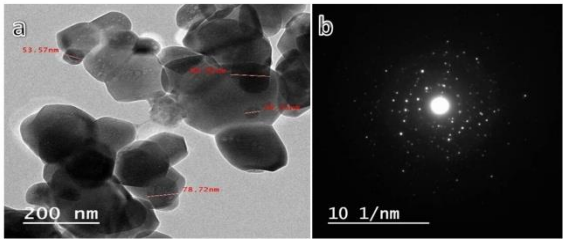

Fig.6. TEM images of calcined nano hydroxyapatite (a), SAED image of calcined nano hydroxyapatite powder (b).

3.1. Characterization of fabricated hydroxyapatite dense bodies

Figure (7) displays the influences of the firing temperature on the bulk density and apparent porosity of the fabricated hydroxyapatite discs. From the result of graph, as the firing temperature increases from 1200^{0}C to 1275^{0}C, the apparent porosity decreases and the bulk density increases due to its grains become more dense packing. Meanwhile, from 1275^{0}C to 1300^{0}C it is found that decrement in the bulk density occurred, it may be assigned to the decomposition of HAp phase to β-TCP [35]. Sintering temperature of HAp was detected at 1275 ^{0}C with the lowest apparent porosity and highest bulk density.

The bulk density has fluctuation phase with change temperature. Accordingly, sintering at 1275^{0}C is the best choice for further investigation; for mechanical and in-vitro tests. The results indicated that the firing temperature influenced the physical properties in terms of apparent porosity and bulk density.

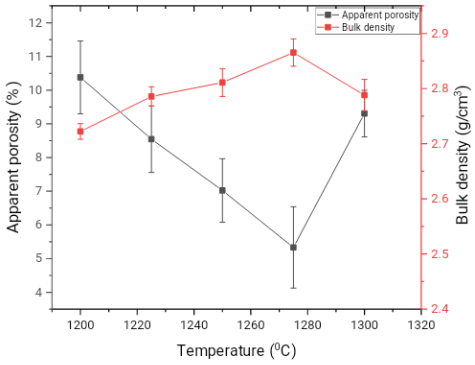

Fig.7. The influence of sintering temperature on the apparent porosity and the bulk density of HAp discs.

Figure (8a) shows the XRD of sintered hydroxyapatite discs sintered at 1275^{0}C for 2h. The XRD diagram indicated that the sintered samples were composed mainly of pure hydroxyapatite JCPDS (009 – 0432) with the appearance of β-tri-calcium phosphate as a secondary phase. The β-TCP was produced as a result of the decomposition of hydroxyapatite at high sintering temperatures (>1200°C) [35]. Numerous studies have suggested the use of HA/-TCP biphasic calcium phosphate composites in bone repair or regeneration because they are more successful than pure phases and have an acceptable rate of biodegradation [62,63].

The SEM micrograph (Fig.8b) demonstrates the microstructure features of the sintered HAp bodies. It shows that the sintered HAp bodies exhibited non-homogeneous sizes for the grains. It was noticed that the polyhedral grains tend to agglomerate. Such grain agglomeration results in the entrapment of pores within grains, thereby accelerating the grain growth. The figure indicates the presence of few β-TCP grains formed due to the high sintering temperature. The XRD diagram confirmed the presence of β-TCP traces in the samples' diagram. The presence of some cracks was also noticed in the sample SEM micrograph. The existing pores had different sizes and shapes, some were rounded, while others with no specific shape.

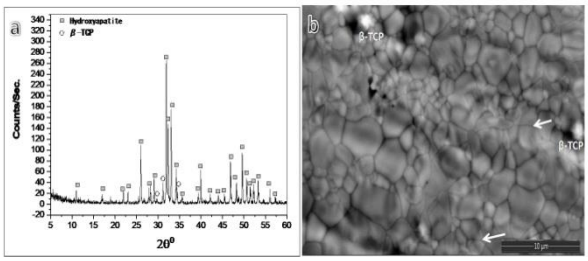

Fig. 8. XRD pattern (a), and SEM (b) of the sintered HAp bodies at 1275°C for 2 h.

The mechanical properties of HAp discs are shown in Table 2. The results reveal that the bending strength value is 38.42± 2.1 MPa and the hardness is 856.35±36.42. It was noticed that the results of the studied samples are relatively low. Lessing the body's grain size is regarded as one of the effectual routes to ameliorate the mechanical properties of ceramic bodies [35], Accordingly with the increase in the grain size the mechanical properties were decreased as shown in the present study. In addition, generally, decreases in the mechanical properties are enhanced by flaws in the ceramic body, such as pores and microcracks (white arrows in Fig. 8b). As pores are areas of stress concentration, the cracks present around such pores are subjected to different levels of stress and together with the existing pores they concentrate stresses and lead to mechanical properties failure [64]. In our next article, we worked on the production of dense hydroxyapatite composites that have high mechanical properties and are suitable for application as a hard bone substitute.

Table. 2: The bulk density, apparent porosity, bending strength, and hardness of HAp discs.

Bulk density, g/cm^3	Apparent porosity, %	Bending strength, MPa	Hardness MPa
2.86 ± 0.02	5.33 ± 1.21	38.73 ± 0.42	856.35±36.42

3.2. In-vitro test

The ICP analysis for the average calcium and phosphorus ions concentrations for the studied sintered hydroxyapatite disks as a function of incubation time in 1.5 SBF (pH 7.4) at 37°C, is demonstrated in Fig. 9a. The results showed that the concentration of calcium ions sharply decreased during the 1st to the 14th incubation day from 140 to 41 mg/l. During the period from the 14th to the 21st days of incubation, an increase in the calcium ions concentration was observed from 41 to 55 mg/l followed by a slight decrease on the 28th of incubation, to reach 54.6 mg/l. On the other hand, the phosphorus ions concentration decreased dramatically from the 1st to the 21st incubation day from 60 to 18.46 mg/l. On the 28th day of incubation, an increase in the phosphorus of 33 mg/l was observed. The above variations in the calcium and phosphorus ions concentration in the SBF solution may be assigned to the development of two phenomena occurring during the incubation period. The first is the apatite particle formation on the sample surfaces, which reduced the concentration of calcium and phosphorus ions. The second is the dissolution process of the examined body, which raises the concentration of calcium and phosphorus ions. The rapid decrease in both calcium and phosphorus ions concentration that was detected in the early incubation period up to the 21st incubation day reveals that

the apatite particle formation rate is higher than the dissolution rate during this period. The apatite particle formation rate decreased with the end of the incubation period after the consumption of most of the calcium and phosphorus ions of the SBF environment and the creation of an apatite layer over the hydroxyapatite disk surface [65].

The in vitro bioactivity evaluation results indicated the pH alteration for the samples immersed for different incubation periods in the 1.5 SBF solution (Fig. 9b). The pH of the SBF solution slightly decreased from 7.44 to 6.88 during the initial day up to the 28th immersion day. The pH decreased as a response to the creation of apatite deposits and the OH^- ions consumption [66].

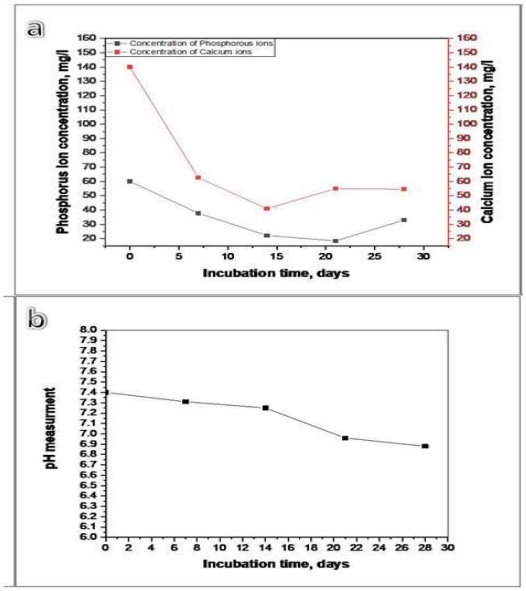

Fig. 9. The changes of the average calcium and phosphorus ions concentration (a), and pH measurements (b) of the sintered HAp samples in 1.5 SBF solution as a function of incubation time.

The ions release of the sintered HAp samples was estimated through immersion of the samples in Tris-HCl buffer solution at different immersion periods ranging between initial to 28 day (Fig. 10a). The Tris-HCl buffer solution was chosen since it does not contain any of the elemental components of the hydroxyapatite phase. The results demonstrated an acute increase in the concentration of the calcium and phosphorus ions detected on the 21st day of immersion. It is due to the dissolution process of the immersed bodies, which is accompanied by positive weight loss values during the incubation period. At the end of the 28th incubation day, a slight decrease in calcium and phosphorus ions concentration took place. This drop is due to apatite particle formation, which consumed these ions and accompanied by negative weight loss % (Fig. 10b).

The degradation behavior of the sintered hydroxyapatite discs was evaluated by measuring their average weight loss% as a function of incubation time in Tris-HCl buffer solution at pH 7.4 and 37°C, Fig. 10b. A sharp increase in weight loss % was detected on the 3rd immersion day equal to 0.24%, followed by lesser increase values during the 7th, 14th and 21st immersion days equal to 0.03, 0.02, and 0.07% respectively. At the end of the 28th incubation day, a weight loss was detected equal to 0.13%, which related to the creation of apatite particles. We believe that low weight loss results are related to the limited amounts of calcium and phosphorus ions released from the sintered HAp discs.

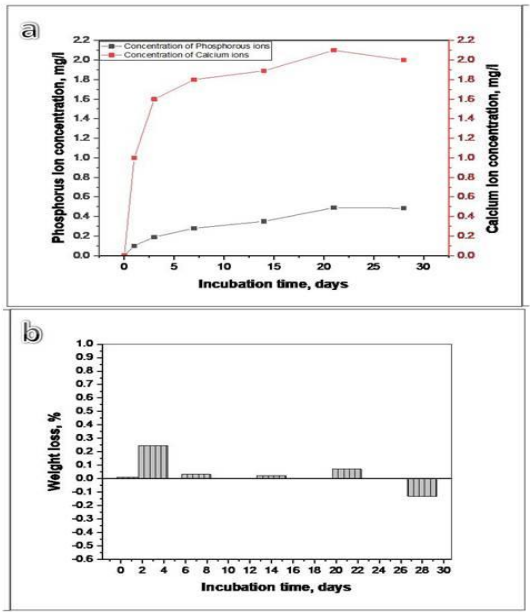

Fig. 10. The changes in the average Ca^{2+} and PO_4^{3-} ions concentration (a) and change in the weight loss % (b) of HAp discs during immersion in Tris-HCl buffer solution as a function of incubation time.

The SEM results of the sintered hydroxyapatite discs after immersion in 1.5 SBF solution for 28 days are illustrated in Figure 11. In comparison with un-immersed HAp samples (Fig. 8b), A highly precipitated dense agglomerated clusters apatite layer appeared over the surface of the studied immersed HAp discs in SBF, Fig. 11. The results pointed out the high surface bioactive of the prepared HAp bodies. Kim, et al., demonstrated that the synthetic HAp promotes bone-like apatite formation on its surface after immersion in SBF solution [67-68]. The bone-like apatite layer formation takes place when the positive calcium ions in the SBF solution interact with the negative ions such as the hydroxyl (OH^-) and phosphate (PO_4^{3-}) groups on the sample's surface, to produce the Ca-rich ACP (amorphous calcium phosphate) and hence, the surface acquires a +ve charge. The formed amorphous calcium phosphate interacts with (-ve) phosphate ions in the SBF solution to produce the Ca-poor ACP. The produced Ca-poor ACP is then crystallized into bone-like apatite in the SBF environment [29].Ca, P and O elements are detected by EDS analysis and the Ca/P ratio was 1.89. The obtained ratio is in the range of 1.2 to 2.2, which is described for amorphous calcium phosphate (ACP) by Dorozhkin (2007) [69].

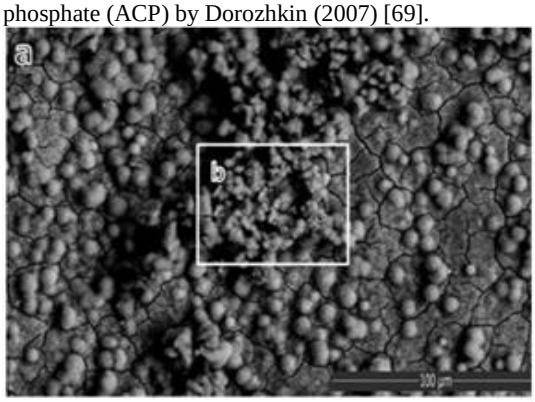

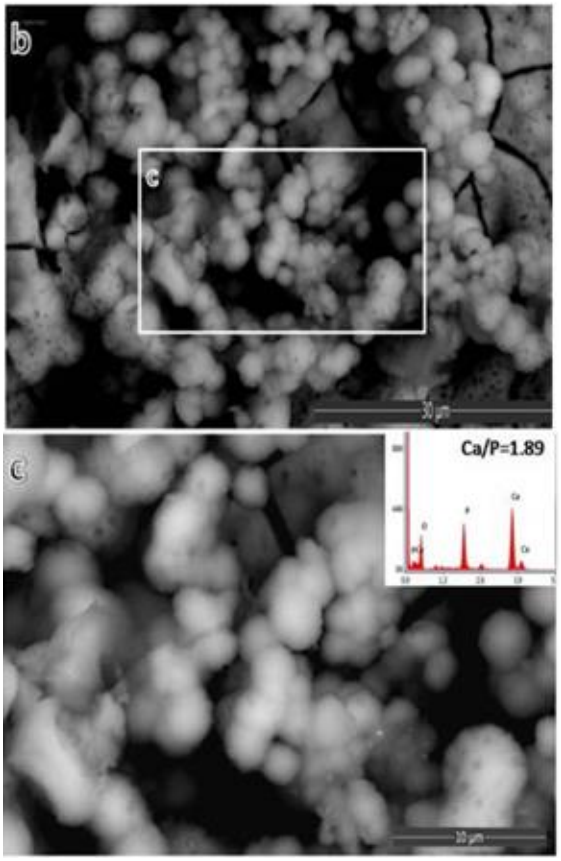

Fig. 11. SEM micrographs and EDS analysis for the surface of the sintered HAp disc after 28 days of immersion in 1.5 SBF solution at different magnifications; (b) and (c) show high magnification of (a) micrograph to show the details of the microstructure.

4. Conclusions

In the present study, nanocrystalline HAp powder was produced from clam shells (Mactridae) as a natural biowaste resource rich with valuable bio-elements. The nano-HAp was fabricated through economical and eco-friendly approaches. Moreover, the obtained nano HAp powder was used to create sintered bodies that mimic the biological activity and structure of the natural bones. The results revealed that:

- The prepared powder comprised pure hydroxyapatite with a particle size meandering between 38.51 and 99.92 nm.
- Due to HAp's partial dissociation and the creation of the β-TCP phase, pure HAp bodies' apparent porosity increases while their bulk density drops as the sintering temperature rises to 1300°C.
- The optimum HAp bodies sintered at 1275°C for 2h possess bending strengths of 38.73 ± 0.4223.66 MPa and Vickers hardness of 856.35±36.42 MPa.
- Based on bioactivity measurements and the in vitro tests, a thick apatite layer was developed on the surface of sintered HAp bodies after 28 days of immersion in 1.5 SBF.

5. Conflicts of interest

There are no conflicts to declare.

6. References

[1] FAO. The State of World Fisheries and Aquaculture 2020. Sustainability in action. FAO; 2020.

[2] N. Yan and X. Chen, "Sustainability: don't waste seafood waste," Nature, vol. 524, no. 7564, 2015, 155–157, DOI: 10.1038/524155a.

[3] J. Zhan, J. Lu, D. Wang. Review of shell waste reutilization to promote sustainable shellfish aquaculture, reviews in aquaculture, 14 [1] 2021, 477-488, DOI: 10.1111/raq.12610.

[4] A. Abeynaike, B. Hanley, L. Wang, M.I. Jones, D.A. Patterson, Investigating the Potential of Using Mussel Shells for the Synthesis of Hydroxyapatite, Chemeca 2008 (36th : 2008 : Newcastle, N.S.W.). Engineers Australia, [Barton, ACT], 2008, 615-629.

[5] Y. Hou, A. Shavandi, A. Carne, A.A. Bekhit, T.B. Ng, R.C.F. Cheung, AE-DA Bekhit. Marine shells: potential opportunities for extraction of functional and health-promoting materials. Crit. Rev. Environ. Sci. Technol. 46, 2016, 1047–1116. DOI:10.1080/10643389.2016.1202669.

[6] A. Abeynaike, L. Wang, M.I. Jones, D.A. Patterson. Pyrolysed powdered mussel shells for eutrophication control: effect of particle size and powder concentration on the mechanism and extent of phosphate removal. Asia-Pacific Journal of Chemical Engineering 6, 2011, 231-243. .DOI:10.1002/apj.426.

[7] H. TAKEYAMA, M. MARUTA, T. SATO, N. KAJIMOTO, E. FUJII, T. MATSUURA, K. TSURU. Fabrication of bioresorbable hydroxyapatite bone grafts through the setting reaction of calcium phosphate cement. Dental material journal, 41,6, 2022, 882-888. DOI:10.4012/dmj.2022-045.

[8] T. Chatterjee, M. Ghosh, M. Maji, M. Ghosh, S. K. Pradhan, A. K. Meikap. Study of microstructural and electrical properties of silver substituted hydroxyapatite for drug delivery applications. Materialstoday communications, 31, 2022, 103360. DOI: 10.1016/j.mtcomm.2022.103360.

[9] A. Farazin& A. Hossein Ghasemi. Design, Synthesis, and Fabrication of Chitosan/Hydroxyapatite Composite Scaffold for Use as Bone Replacement Tissue by Sol–Gel Method. Journal of Inorganic and Organometallic Polymers and Materials, 32, 2022, 3067-3082. DOI:10.1007/s10904-022-02343-8

[10] N. Rezania, M. Asadi-Eydivand, N. Abolfathi, S. Bonakdar, M. Mehrjoo, M. Solati-Hashjin. Three-dimensional printing of polycaprolactone/hydroxyapatite bone tissue engineering scaffolds mechanical properties and biological behavior. Journal of Materials Science: Materials in Medicine. 33, 312022, 1-14. DOI: 10.1007/s10856-022-06653-8.

[11] N. Elizondo-Villarreal, A. Martínez-de-la-Cruz, R.O. Guerra, J.L. Gomez-Ortega, L.M. Torres-Martínez, V.M. Castano, Biomaterials from agricultural waste: eggshell based hydroxyapatite, Water Air Soil Pollut. 223, 2012, 3643-3646. DOI: 10.1007/s11270-012-1137-1.

[12] S.-C. Wu, H.-C. Hsu, Y.-N. Wu, W.-F. Ho, Hydroxyapatite synthesized from oyster shell powders by ball milling and heat treatment, Mater. Charact. 62, 2011, 1180-1187. DOI: 10.1016/j.matchar.2011.09.009.

[13] Y. AZIS, N. JAMARUN, S. ARIEF, H. NUR, Facile Synthesis of Hydroxyapatite Particles from Cockle Shells (Anadaragranosa) by Hydrothermal Method, Oriental Journal of Chemistry, 31, [2], (2015), 1099-1105. DOI: 10.13005/ojc/310261

[14] A. Teymouri, B. J. Stuart, S. Kumar, Hydroxyapatite and dittmarite precipitation from algae hydrolysate, , Algal Research, 29, 2018 ,202-211. DOI: 10.1016/j.algal.2017.11.030.

[15] O. Gunduz, A Simple Method of Producing Hydroxyapatite and Tri Calcium Phosphate from Coral (Pocilloporaverrucosa), J. Australian Ceram. Soc., 50(2), 2014, 52-58.

[16] N. A.M. Barakat, M. SeobKhil, A.M. Omrand, F. A. Sheikhd, H. Y. Kim, Extraction of pure natural hydroxyapatite from the bovine bones bio waste by three different methods, journal of materials processing technology 209, 2009, 3408–3415. DOI: 10.1016/j.jmatprotec.2008.07.040.

[17] R. Chakraborty, D. RoyChowdhury, Fish bone derived natural hydroxyapatite supported copper acid catalyst: taguchi optimization of semibatch oleic acid esterification, Chem. Eng. J. 215-216, 2013, 491-499. DOI: 10.1016/j.cej.2012.11.064.

[18] I. Sukmana, A. Hendriyanto, S. Savetlana, and Tarkono, The effect of sintering parameter on the properties of hydroxyapatite from local limestone for bone implant application, 1977, 2018, 1,030039. DOI: 10.1063/1.5042959.

[19] B.A. Allo, A.S. Rizkalla, K. Meuanint, Hydroxyapatite formation on sol-gel derived poly (epsilon-caprolactone)/bioactive glass hybrid biomaterials, ACS Appl. Mater. Interfaces. 4(6), 2012, 3148-3156. DOI: 10.1021/am300487c.

[20] A.F. Lemos, J.H.G. Rocha, S.S.F. Quaresma, S. Kannan, F.N. Oktar, S. Agathopoulos, J.M.F. Ferreira, Hydroxyapatite nano-powders produced hydrothermally from nacreous material, J. Eur. Ceram. Soc., 26 [16], 2006, 3639-3646. DOI: 10.1016/j.jeurceramsoc.2005.12.011.

[21] Ahmed M Bakr, Badwi Anis, Walid El hotaby, sounchemical synthesis of graphene/ nano hydroxyapatite composites for potential biomedical application, Egyptian Journal of Chemistry,65,2022, 2,669-678.Doi:10.21608/ejchem.2021.91241.4339.

[22] A. Shavandi, A. El-Din, A. Bekhit, A. Ali, Z. Sun. Synthesis of nano hydroxyapatite (nHA) from waste mussel shells using a rapid microwave method, Mater. Chem. Phys., 149-150, 2015, 607-616. DOI: 10.1016/j.matchemphys.2014.11.016.

[23] G.K. Lim, J. Wang, L.M. Gan, Processing of fine hydroxyapatite powders via an inverse micro emulsion route, Mater. Lett.,1996, 30, 431-433. DOI: 10.1016/0167-577X (96)00095-X.

[24] B. Yeong, X. Junmin, J. Wang, Mechanochemical synthesis of hydroxyapatite from calcium oxide and brushite, J. Am. Ceram. Soc., 84, 2004, 465-467. DOI: 10.1111/j.1151-2916. 2001.tb00681.x.

[25] S. Yang, J. Chen, Z. Wang, H. Zhang, Q. Zhang, Surfactant assisted synthesis of oriented hydroxyapatite nanocluster by reflux method, Mater. Lett. , 96, 2013, 177-180. DOI: 10.1016/j.matlet.2013.01.062.

[26] Y. Han, T. Fu, J. Lu, K. Xu. Characterization and stability of hydroxyapatite coatings prepared by an electrodeposition and alkaline-treatment process, J Biomed Mater Res. 54 [1], 2001, 1-148. DOI: 10.1002/1097 4636(200101)54:1<96::aid-jbm11>3.0.co;2-u .

[27] P. Rouhani, N. Taghavinia, S. Rouhani. Rapid growth of hydroxyapatite nanoparticles using ultrasonic irradiation, Ultrasonics Sonochemistry, 17 [5], 2010, 853-856. DOI: 10.1016/j.ultsonch.2010.01.010.

[28] N.Eliaz, N. Metoki. Calcium Phosphate Bioceramics: A Review of Their History, Structure, Properties, coating Technologies and Biomedical Applications. Materials. 10, 2017, 334. DOI: 10.3390/ma10040334.

[29] S. Rujitanapanich, P. Kumpapan, P. Wanjanoi. Synthesis of hydroxyapatite from oyster shell via precipitation. Energy Proc, 56: 2014, 112–117. DOI: 10.1016/j.egypro.2014.07.138.

[30] M. Sadat-Shojai, M.T. Khorasani, E. Dinpanah-Khoshdargi, A. Jamshidi. Synthesis methods for nanosized hydroxyapatite with diverse structures. Acta Biomater, 9 [8], 2013, 7. DOI: 10.1016/j.actbio.2013.04.012.

[31] G.M. Raghavendra, K. Varaprasad, T. Jayaramudu,in: S. Thomas, Y. Grohens, N. Ninan (Eds.), Chapter 2 - biomaterials: design, development and biomedical applications, Nanotechnology Applications for Tissue Engineering, William Andrew Publishing, Oxford, 2015, 21–44. DOI:10.1016/B978-0-323-32889-0.00002-9.

[32] J.S. Temenoff, A.G. Mikos, Biomaterials: The Intersection of Biology and Materials Science, Pearson/Prentice Hall, 2008.

[33] N. Lertcumfu, P. Jaita, S. Manotham, P. Jarupoom, S. Eitssayeam, K. Pengpat, G. Rujijanagul, Properties of calcium phosphates ceramic composites derived from natural materials, Ceram. Int., 42, 2016, 10638–10644. DOI: 10.1016/j.ceramint.2016.03.162

[34] M.H. Fathi, A. Hanifi, V. Mortazavi. Preparation and bioactivity evaluation of bone-like hydroxyapatite nanopowder. J Mater Process Technol. 202 (1) 2008, 536–542. DOI: 10.1016/j.jmatprotec.2007.10.004

[35] S.M. Naga, M. Sayed, H.F. El-Maghraby. Physicomechanical, Phasese composition and In Vitro study of high temperature sintered ZTA/HA composites. Metallurgical and Materials Transactions A. 50, 2019, 5533-5541. DOI: 10.1007/s11661-019-05433-4.

[36] M. Blum, M. Sayed, E.M. Mahmoud, A. Killinger, R. Gadow, S.M. Naga. In Vitro Evaluation of Biologically Derived Hydroxyapatite Coatings Manufactured by High Velocity Suspension Spraying. J Thermal Spray Technology 30 (2021)1891–1904. DOI:10.1007/s11666-021-01265-0.

[37] X. Y.Guo and P.Xiao. Fabrication of Nanostructured Hydroxyapatite via Hydrothermal Synthesis and Spark Plasma Sintering, J. Am. Ceram. Soc., 2005, 881026–1029. DOI: 10.1111/j.1551-2916.2005. 00198.x.

[38] S. Bose, S. Dasgupta, S. Tarafder, and A. Bandyopadhyay. Microwave-Processed Nanocrystalline Hydroxyapatite: Simultaneous Enhancement of Mechanical and Biological Properties,ActaBiomater., 6(9), 2010, 63782– 3790. DOI: 10.1016/j.actbio.2010.03.016.

[39] I. W. Chen and X. H. Wang. Sintering Dense Nanocrystalline Ceramics without Final-Stage Grain Growth, Nature, 404, 2000, 168– 171. DOI: 10.1038/35004548.

[40] K. Dhanaraj, G. Suresh, Vacuum, Conversion of waste sea shell (Anadaragranosa) into valuable nanohydroxyapatite (nHAp) for biomedical applications, Vaccum, 152, 2018, 222-230. DOI: 10.1016/j.vacuum.2018.03.021

[41] M. Zulhasif Ahmad Khiri, K. Amin Matori, M. Hafiz Mohd Zaid, Che Azurahanim Che Abdullah, N. Zainuddin, I. Mustapha Alibe, N. Asyikin Abdul Rahman, S. Aisyah Abdul Wahab. The effect of the pH values and sintering temperatures on the physical, structural and mechanical properties of nano hydroxyapatite derived from ark clam shells (Anadara Granosa) prepared via the wet chemical precipitate method, Ceramics-Silikáty. 63 (2), 2019, 194-203. DOI:10.13168/cs.2019.0011.

[42] G. Karunakaran, E.B. Cho, G. S. Kumar, E. Kolesnikov, G. Janarthanand M. M. Pillai, S. Rajendran, S. Boobalan, K. G. Sudha, M. P. Rajeshkumar. Mesoporous Mg-doped hydroxyapatite nanorods prepared from bio-waste blue mussel shells for implant applications. Ceramics International. 46 [18] Part A, 2020, 28514-28527. DOI: 10.1016/j.ceramint.2020.08.009.

[43] S. Hussain, K. Sabiruddin, Effect of heat treatment on the synthesis of hydroxyapatite from Indian clam seashell by hydrothermal method. Ceramics International. 47, 21, 2021, 29660-29669. DOI: 10.1016/j.ceramint.2021.07.137

[44] M. Harkat, S. Alleg, R. Chemam, N. Moutia, K. Khirouni, E. Dhahri. Structure and Electric Characterizations of the Derived Nanocrystalline Hydroxyapatite from Strombidae Strombus Seashells. Arabian Journal for Science and Engineering, 47, 2022, 7693–7706. DOI:10.1007/s13369-021-06556-w.

[45] H. A. El Mekawy, A. A. M. El-Sayed, M. A. Amer, M. M. H. Sarhan. Revision of Families Veneridae and Mactridae (Mollusca: Bivalvia) From the Suez Gulf, Egypt. Egypt. Acad. J. Biolog. Sci., 11[2], 2019, 65- 97. DOI: 10.21608/eajbsz.2019.42092

[46] ASTM C-20; Standard Test Methods for Apparent Porosity, Water Absorption, Apparent Specific Gravity, and Bulk Density of Burned Refractory Brick and Shapes by Boiling Water.

[47] T. Kokubo, H. Kushitani, S. Sakka, T. Kitsugi, T. Yamamuro, Solutions able to reproduce in vivo surface-structure changes in bioactive glass-ceramics A-W, J. Biomed. Mater., Res. 24, 1990, 721–734. DOI: 10.1002/jbm.820240607.

[48] EN-ISO-10993-14. Biological evaluation of medical devices - Part 14: Identification and quantification of degradation products from ceramics. ISO 10993-142001. 2001.

[49] Abeer M El-Kady, E. M. Mahmoud, M. Sayed, S.M. Kamel, S.M. Naga, In-vitro and In-vivo evaluation for the bio-natural Alginate/Nano- Hydroxyapatite (Alg/n-HA) injectable hydrogel for critical size bone substitution. International Journal of Biological Macromolecules, 253, 1, 2023, 126618. DOI: 10.1016/j.ijbiomac.2023.126618.

[50] S.K. Arepalli, H. Tripathi, V. K. Vyas, S. Jain, S. K. Suman, R. Pyare, S.P. Singh, Influence of barium substitution on bioactivity, thermal and physico-mechanical properties of bioactive glass, Materials Science and Engineering: C, 49, 2015, 549-559. DOI:10.1016/j.msec.2015.01.049.

[51] Y. Chen, SI. Roohani-Esfahani, Z. Lu, H. Zreiquat, CR. Dunstan. Zirconium ions up-regulate the BMP/SMAD signaling pathway and promote the proliferation and differentiation of human osteoblasts. PLoS One. 2015; 10: e0113426. DOI:10.1371/journal.pone.0113426

[52] T. Tanaka, I. Kojima, T. Ohse, J.R. Ingelfinger, S. Adler, T. Fujita, M. Nangaku, Cobalt promotes angiogenesis via hypoxia-inducible factor and protects tubulointerstitium in the remnant kidney model, Laboratory Investig., 85 [10], 2005, 1292–1307. DOI: 10.1038/labinvest.3700328.

[53] W. Fan, R. Crawford, Y. Xiao. Enhancing in vivo vascularized bone formation by cobalt chloride-treated bone marrow stromal cells in a tissue engineered periosteum model, Biomaterials, 31 [13] , 2010, 3580–3589. DOI: 10.1016/j.biomaterials.2010.01.083.

[54] Y. Pu, H. Sun, J. Liu, D. Amantai, W. Yao, X. Han, H. He. Cobalt Chloride Promotes Osteogenesis of Rat Bone Marrow Mesenchymal Stem Cells In Vitro and In Vivo. Indian J. Pharm Sci. 85, 2023, 1–10. **DOI**: 10.36468/pharmaceutical-sciences.spl.635.

[55] Standard Specification for Glass and Glass Ceramic Biomaterials for Implantation, ASTM International, West Conshohocken, PA, USA, 2003, 1–4.

[56] B.D. Cullity, S.R. Stock, Elements of X-Ray Diffraction (Prentice Hall, 2001).

[57] N. Nordin, Z. Hamzah, O. Hashim, F.Hafiz Kasim, R. Abdullah. Effect of temperature in calcinations process of seashells. Malaysian Journal of Analytical Sciences. 19 [1] 2015, 65 – 70.

[58] M. Okada, K. Fujiwara, M. Uehira, N. Matsumoto, S. Takeda. Expansion of nanosized pores in low-crystallinity nanoparticle-assembled plates via a thermally induced increase in solid-state density, J. Colloid Interface Sci., 405, 2013, 58–63. DOI: 10.1016/j.jcis.2013.05.022.

[59] Y. Azis, N. Jamarun, S. Arief, H. Nur. Facile synthesis of hydroxyapatite particles from cockle shells (Anadaragranosa) by hydrothermal method. Orient J Chem. 31[2], 2015;. DOI:10.13005/ojc/310261.

[60] C. Suresh Kumar, K. Dhanaraj, R.M. Vimalathithan, P. Ilaiyaraja& G. Suresh. Hydroxyapatite for bone related applications derived from sea shell waste by simple precipitation method, Journal of Asian Ceramic Societies, 8:2, 2020, 416-429. DOI:10.1080/21870764.2020.1749373.

[61] J. S. Zuluaga-Morales , M. V. Bolaños-Carmona , C. C. Cifuentes-Jiménez and P. Álvarez-Lloret. Chemical, Microstructural and Morphological Characterisation of Dentine Caries Simulation by pH-Cycling .Minerals, 12(5), 2022, 1-16. DOI:10.3390/min12010005.

[62] Ryu, H.S. Youn, H.J. Hong, K. S. Chang, B.S. Lee, C. K. and Chung S.S. An improvement in sintering property of β-tricalcium phosphate by addition of calcium pyrophosphate. Biomaterials, 23, 2002, 909–914. DOI: 10.1016/s0142-9612(01)00201-0.

[63] S.H. Kwon, Y.K. Jun, S.H. Hong, and H.E. Kim, Synthesis and Dissolution Behavior of β-TCP and HA/β-TCP Composite Powders. Journal of the European Ceramic Soc., 23, 2003, 1039-1045. DOI:10.1016/S0955-2219(02)00263-7.

[64] S.M. Naga, H.F. El-Maghraby, M. Elgamhoudy, M.A. Saleh. Characterization and origin of failure of SiC/ZTA composites. Int J Refract Hard Met., 73, 2018, 53-57. DOI:10.1016/j.ijrmhm.2018.01.016.
[65] M. Sayed, E.M. Mahmoud, S.M. Saber, S. N. Raafat, S.M.Gomaa, S.M. Naga. Effect of the injectable alginate/ nano-hydroxyapatite and the silica/ nano-hydroxyapatite composites on the stem cells: a comparative study. Journal of Non-Crystalline Solids, 610, 2023, 122327.DOI: 10.1016/j.jnoncrysol.2023.122327.
[66] R. V. Suganthi, S. Prakash Parthiban, K. Elayaraja, E. K. Girija,P.Kulariya, Y. S. Katharria, F. Singh, K. Asokan, D. Kanjilal, S. Narayana Kalkura. Investigations on the in vitro bioactivity of swift heavy oxygen ion irradiated hydroxyapatite. J Mater Sci: Mater Med, 20, 2009, S271–S275. DOI: 10.1007/s10856-008-3652-6.
[67] H.-M. Kim, T. Himeno, M. Kawashita, T. Kokubo, T. Nakamura. The mechanism of biomineralization of bone-like apatite on synthetic hydroxyapatite: an in vitro assessment, J. R. Soc. Interface, 1[1], 2004, 17-22. DOI:10.1098/rsif.2004.0003.
[68] S. Itoh, S. Nakamura, T. Kobayashi, K. Shinomiya, K. Yamashita, S. Itoh. Effect of electrical polarization of hydroxyapatite ceramics on new bone formation,Calcif. Tissue Int., 78 [3], 2006, 133-42. DOI:10.1007/s00223-005-0213-6.
[69] Dorozhkin S.V. Bioceramics based on calcium orthophosphates. (Review) Glass Ceram. 64 (11-12), 2007, 442-447. DOI:10.1007/s10717-007-0109-1.